JOURNAL OF MATERIALS SCIENCE 20 (1985) 736–755

Load relaxation studies of germanium

S.-W. CHIANG*, D. L. KOHLSTEDT
Department of Materials Science and Engineering, Cornell University, Ithaca, NY 14853, USA

A series of compressive load relaxation experiments were conducted on germanium single crystals in the temperature range 400 to 885° C. The curvature of the log σ–log $\dot{\epsilon}$ data obtained from load relaxation tests changes from concave upward to concave downward as the test temperature increases at fixed stress level, or as the strain level increases at fixed temperature. At intermediate temperatures, ~600° C, the transition from concave upward to concave downward curvature happens on a single relaxation curve. These observations are consistent with the two-branch rheological model proposed by Hart to explain the deformation behaviour of metals and were analysed in terms of this model. The transition from concave upward to concave downward curvature could be moved to higher temperature by doping germanium with gallium, which decreases the dislocation glide velocity relative to that in pure germanium. The transition could be shifted to lower temperature by compressing samples along $[1\bar{1}1]$ rather than $[1\bar{1}0]$ because the $[1\bar{1}1]$ orientation favours cross-slip while the $[1\bar{1}0]$ orientation does not. Dislocation dipoles and straight dislocations dominated the microstructure of samples which had concave upward log σ–log $\dot{\epsilon}$ curves, while well-developed dislocation cell structures dominated the microstructure of samples which yielded concave downward curves. The observed changes in the curvature of the load relaxation curves and the dislocation structure both indicate the increased importance of dislocation climb with increasing temperature. When compared through the Orowan equation, the load relaxation results are in good agreement with published stress–dislocation velocity data.

1. Introduction

The properties of dislocations under stress and the role of dislocations in the mechanical behaviour have been widely studied in crystalline materials. Deformation experiments have been performed on single crystals and polycrystals to investigate the relationships among stress, temperature, dislocation velocity, strain rate, and microstructure. Such studies are particularly promising in semiconducting materials such as germanium and silicon because impurity effects can be ignored due to their high as-grown perfection. Also, dislocations introduced by deformation at high temperatures are nearly immobile at room temperature. Thus, dislocation structures in these diamond cubic materials are not altered during sample preparation.

The stress–dislocation velocity data for germanium and silicon has generally been interpreted in terms of models of undissociated dislocations [1]. In these models, kink formation on and kink migration along dislocation lines control the glide at low temperature for these crystals which have high Peierls stresses [2]. A few measurements of dislocation velocity have been reported for germanium [1, 3, 4] at temperatures below 2/3 T_m, where T_m is the melting temperature. At temperatures above 0.6 T_m, constant strain-rate and creep tests have been used to investigate the stress–dislocation velocity relations [5, 6]. One of the purposes of the present work is to utilize load relaxation tests to deform germanium crystals at 0.56 to 0.96 T_m in order to study the possible dislocation mechanisms over large ranges of temperature and strain rate.

*Present address: IBM East Fishkill, Hopewell Junction, NY 12533, USA.

0022–2461/85 $03.00 + .12

Weak-beam transmission electron microscopy [7] reveals that dislocations in deformed germanium and silicon are dissociated into partial dislocations [8–11]. Direct observations demonstrate that dislocations can glide in the dissociated configuration [12]. However, the effects of dislocation dissociation and the energy of the associated stacking fault on the mobility of these dislocations need more consideration in terms of kink mechanisms [13].

A single power-law relationship between dislocation velocity and effective stress does not describe the experimental data at constant temperature [3, 4]. However, Möller [14] has recently proposed a model for the movement of dissociated dislocations in crystals with both a high Peierls potential and weak obstacles. The mean separation between weak obstacles on a dislocation is about $1\,\mu m$ ($T = 0.6\,T_m$). He assumed that constrictions along dissociated dislocations are these weak obstacles. His model predicts a step in the stress–dislocation velocity curve for germanium. Although this model adequately describes the existing stress–dislocation velocity data, experimental data at lower stresses and/or at $T > 2/3\,T_m$ are needed to test his model further.

Möller [14] used a mechanistic approach to develop equations to describe the mechanical behaviour of germanium. In an alternative approach, phenomenological theories of mechanical behaviour have recently been developed to describe deformation in metals [15]. The aim of the present study is to explore the mechanical behaviour of germanium from the state-variable point-of-view [16] and to study its relationship to dislocation structures observed in the deformed crystals and to dislocation velocity–stress data reported in the literature. Thus, the mechanical properties of germanium single crystals deformed over a large temperature range are described in terms of a mechanical equation-of-state. Transmission electron microscopy (TEM) observation on the deformation-induced dislocation structures and the results of load relaxation tests are used to investigate the relation between a macroscopic state parameter and the dislocation structures. In addition, the effects of the orientation of the specimen relative to the compression axis and of doping on dislocation cross-slip and dislocation velocity, respectively, are analysed.

2. Experimental details

2.1. Deformation tests

2.1.1. Materials and sample preparation

Both high-purity and gallium-doped germanium single crystals* were tested. The high-purity crystals had room-temperature resistivity greater than 40 ohm cm, which corresponds to a concentration of electrical active impurities of $\sim 2 \times 10^{13}$ cm^{-3}. The gallium-doped crystal had a doping level of $\sim 2 \times 10^{19}\,cm^{-3}$. The as-received dislocation densities in both types of crystals were $\sim 2 \times 10^3\,cm^{-2}$.

Specimens were oriented with either a $[1\bar{1}0]$ compression axis and $(11\bar{1})$ and (112) lateral faces or a $[1\bar{1}1]$ compression axis and $(\bar{1}01)$ and (121) lateral faces by the Laue back-reflection technique. At the start of a deformation test for the $[1\bar{1}0]$ compression samples, the Schmid factor for four of the $\{111\}\langle 1\bar{1}0\rangle$ slip systems is 0.41; for the $[1\bar{1}1]$ compression samples, the Schmid factor for six of the $\{111\}\langle 1\bar{1}0\rangle$ slip systems is 0.27.

After a final mechanical polish with $0.3\,\mu m$ alumina powder, the specimens used in most of the experiments were predeformed at 600° C to ~ 1.2% strain, relaxed for 20 min, and then annealed at 800° C for 3 h. This treatment generated a uniform dislocation distribution with a starting dislocation density of $\sim 10^7\,cm^{-2}$. An optical micrograph of the starting dislocation structure revealed by etching is shown in Fig. 1.

2.1.2. Experimental apparatus and procedure

The experimental apparatus was similar to that used previously in our laboratory for room-temperature runs [17]. Essential details of the experimental procedure and modifications for testing at elevated temperatures are described here. Specimens were deformed in compression in the temperature range 400 to 885° C in one atmosphere of argon passed through a getter containing hot (~ 750° C) Ti chips. The test temperatures were obtained with a tungsten-mesh heating element which was housed in a water-cooled chamber. A screw-driven testing machine was used at constant crosshead velocity to generate a specimen strain rate of $\sim 2.6 \times 10^{-4}\,sec^{-1}$. After the sample was deformed to a predetermined strain or stress level, the crosshead was held fixed. The load against time data during each loading and

*Purchased from Eagle-Pricher Industries, Quapaw, Oklahoma 74363.

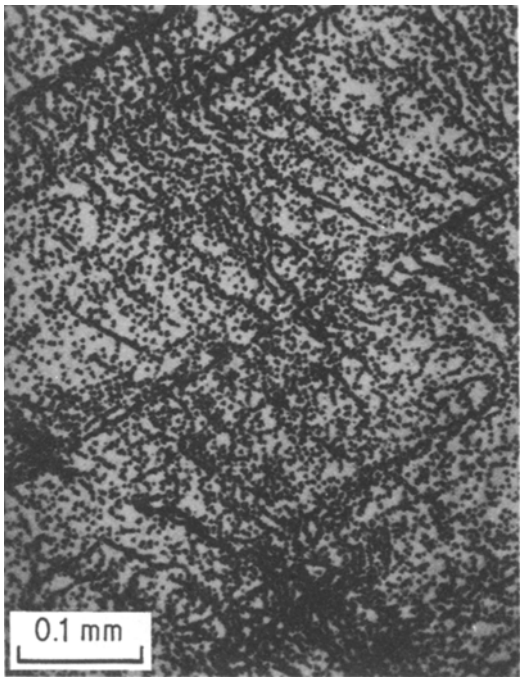

Figure 1 Dislocation etch-pits on a (1 1 1) surface showing the starting dislocation structure in predeformed and annealed germanium samples.

relaxation run were recorded digitally on magnetic tape. The rate of data collection was changed several times during the course of run. For the first two minutes, ten data points were recorded per second; for the next twenty minutes, one data point was recorded per second; for the remainder of the run (~ 100 min), one data point was collected every 50 sec. The load–time data were later analysed on a computer to obtain stress–strain and stress–strain rate results. The details of this data processing have been described previously [17–19].

A stable temperature is essential in order to minimize thermal expansion effects in the testing machine and load train sufficiently to obtain data at strain rates below 10^{-6} sec^{-1} ($t \gtrsim 5$ min). The temperatures of the furnace, room, and cooling water for the furnace chamber and pistons were controlled to $\pm 0.1^{\circ}$ C over a 24 h period. A steady-state temperature was reached by operating the furnace for at least eight hours prior to the testing. The testing machine was turned on only for the short time required to load the specimen so as to minimize the heat generated from the motors.

Five modifications were made to reduce the relaxation of the machine and load train. On the testing machine, the two condensers in the damping network were shorted out, the preload springs on top of the drive screws were tightened, and the grease between the crosshead and the drive screws was removed. All of the connections in the load train, including those between the high-strength graphite pistons and the thoriated-tungsten platens, were tightened under load. The specimen size was chosen so that the load level exceeded 70 kg; above approximately 40 kg, all components in the load train were firmly seated as evidenced by the linear load–displacement curves obtained with a stiff sample. Less than 5% of the total load drop during a relaxation run can be attributed to thermal fluctuations and machine relaxation.

2.2. Microstructural observations

Two methods were used to study dislocation structures in germanium, optical examination of dislocation etch pits on {1 1 1} surfaces and transmission electron microscope observation of dislocations in thin foils. The procedure for producing dislocation etch pits was modified from the method suggested by Billig [20]. The {1 1 1} surface of germanium crystals were mechanically polished to remove all scratches visible optically at × 500. The specimens were chemically polished by immersion for 30 sec in $HNO_3 + H_2O + HF$ acid bath of volume ratio of 5:1:1. Optically distinct etch pits were then readily produced by etching for one to four minutes in a boiling solution of 8 g $K_3Fe(CN)_6$ + 12 g KOH + 100 ml H_2O.

Oriented thin-foils for transmission electron microscopy were prepared from slices which had been mechanically ground and polished to a thickness of less than 50 μm. These slices were thinned further in a 9:1 solution of HNO_3 and HF until a small hole appeared near the center of the foil. The TEM foils were examined on a Siemens 102 electron microscope operating at 125 kV.

3. Experimental results

Stress–strain curves, log stress–log strain rate curves, and dislocation structures resulting from compressive deformation tests on germanium are described in this section.

3.1. Stress–strain data

The true stress–true inelastic strain curves for high-purity germanium single crystals compressed along [1 $\bar{1}$ 0] at four temperatures during both

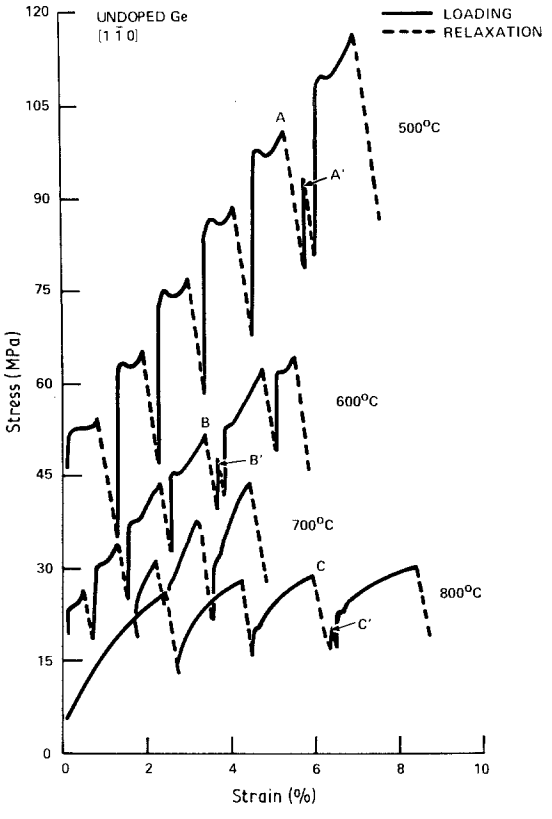

Figure 2 True stress–inelastic strain curves at four temperatures for germanium single crystals compressed along [1 1̄ 0]. Samples were loaded at a strain rate of about 2.6×10^{-4} sec^{-1}.

constant loading rate and load relaxation tests are shown for four temperatures in Fig. 2. The predeformation treatment described in the previous section eliminated the pronounced yield drop usually associated with the stress–strain curves of ionic and covalent solids with low starting dislocation densities [21, 22]. A small yield drop occurred during each loading at 500 and 600° C. After the first loading, the magnitudes of the yield drop were approximately constant (independent of strain). The yield drops at 500° C were larger than those at 600° C. At 700 and 800° C, the magnitudes of the yield drop increased with increasing strain; a saturation value may be reached at strain levels higher than those explored here. The magnitude of the yield drop decreased with increasing temperature.

At 500° C, the lower yield point of a reloading run was higher than the peak stress reached immediately before the preceding load relaxation test. The difference between these two stresses was approximately independent of strain. At 600° C, the reloading lower yield point is above the previous peak stress for strains $< 3\%$, but it is below the previous peak stress for strains $> 3\%$. At 700 and 800° C upon reloading, the crystal yielded at a lower stress than the peak stress of the preceding run.

In load relaxation tests, the stress decreased approximately 20 to 30% in 2 h. The strain increments during load relaxation were always less than 0.5%.

Supplementary experiments were performed to expand the above observations with particular attention to the question, "does the crystal harden or soften during a relaxation run?" Fig. 3 shows load against time data for a series of constant compression-rate, relaxation, and static annealing runs at 500 and 800° C on crystals which had been predeformed and annealed. The following points can be made. At 500° C: (a) the yield drop after a one hour static anneal or load relaxation test is larger than that observed when the sample is unloaded and immediately reloaded. (b) The difference between the lower yield point and the previous peak stress is about the same whether the sample is (i) immediately reloaded or (ii) relaxed and then reloaded. This difference decreases, if the sample is statically annealed before reloading. At 800° C: (a) upon reloading, the yield point always lies below the previous peak stress. (b) The reloading yield point is above that of the previous loading, if the sample is immediately reloaded, and is below that of the previous loading, if the sample is first relaxed.

3.2. Stress–strain rate data

The log σ–log $\dot{e}$ curves for high-purity germanium crystals deformed along [1 1̄ 0] were calculated from the load relaxation results obtained at temperatures between 400 and 885° C. Data at 400, 440, 500, 600, 700 and 800° C are presented in Figs. 4 to 9. The shape and curvature of the log σ–log $\dot{e}$ curves vary systematically with increasing temperature and deformation history.

The three log σ–log $\dot{e}$ curves at 440° C, Fig. 5, are concave upward. The slopes of these curves at a given strain rate decrease as stress increases. These results are similar to those observed for metals [23–27] and alkali halides [17–19] at low homologous temperatures.

The data from the load relaxation experiments performed at 400° C exhibited an anomalous behaviour. Two log σ–log $\dot{e}$ curves for a chemically

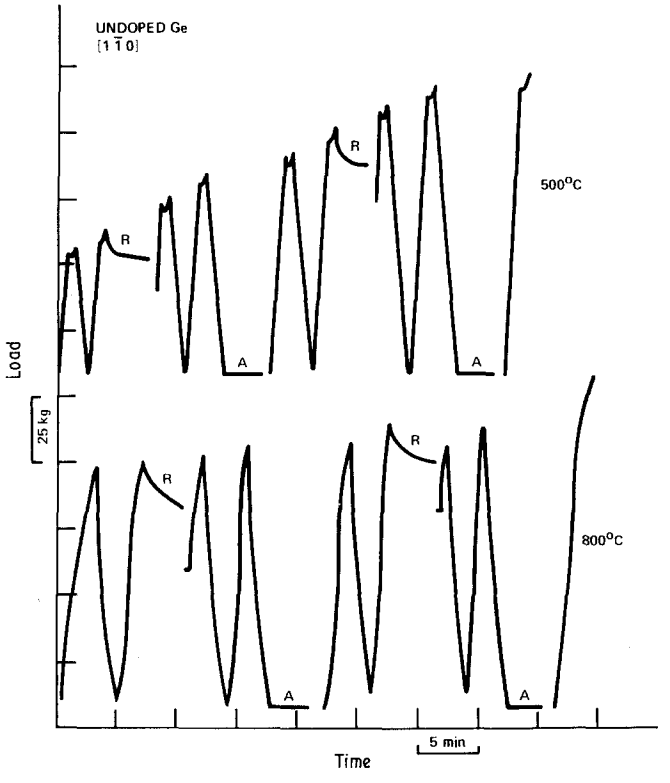

Figure 3 Load–time history for germanium crystals compressed along [1$\bar{1}$0] at 500 and 800° C. The effects of both static annealing, A, and load-relaxation, R, on the reloading behaviour were examined.

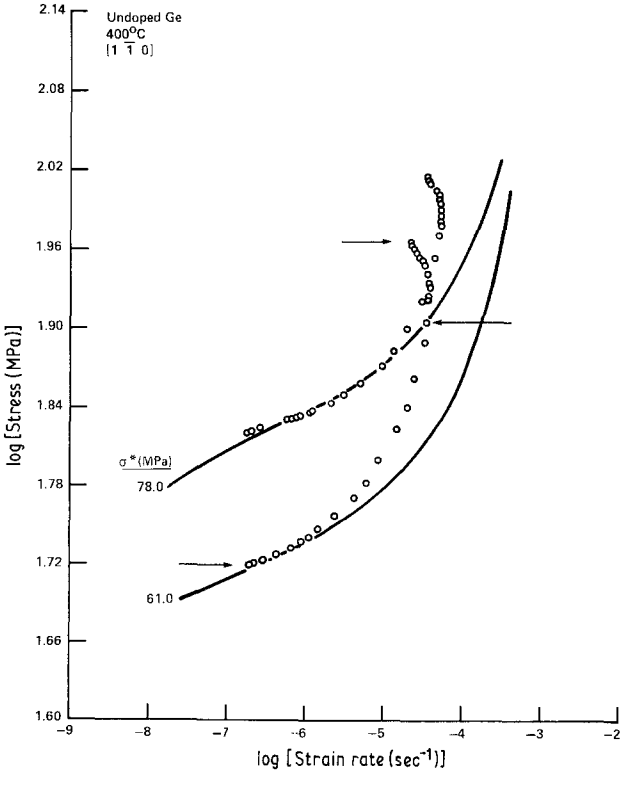

Figure 4 Log σ–log $\dot{\epsilon}$ data obtained from load relaxation experiments at two plastic strain levels for a high-purity germanium crystal compressed along [1$\bar{1}$0] at 400° C. The solid curves are a fit of the data to the constitutive equations discussed in the text. The arrows indicate points at which load relaxation runs were stopped in order to examine the dislocation structure.

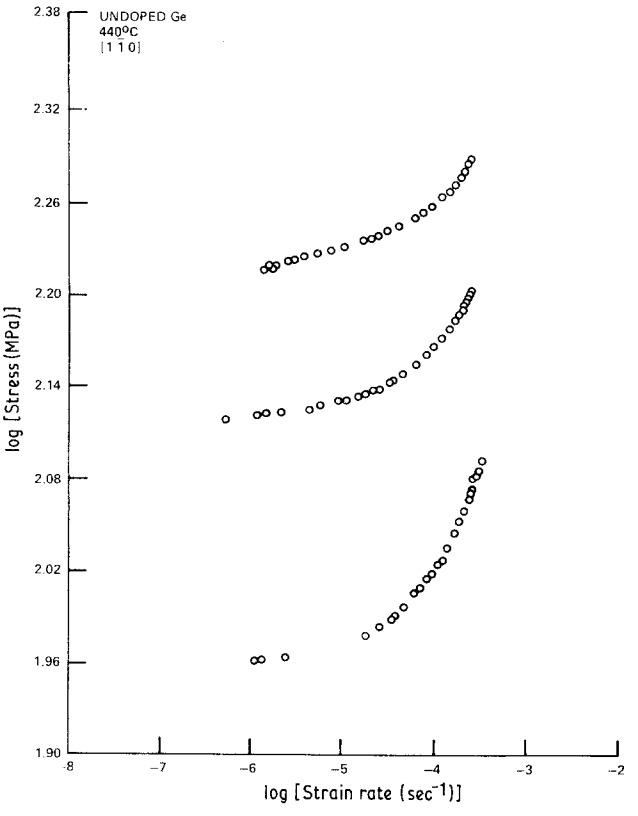

Figure 5 Log σ–log $\dot{\epsilon}$ data obtained from load relaxation experiments at three plastic strain levels for a high-purity germanium crystal compressed along $[1\bar{1}0]$ at 440° C.

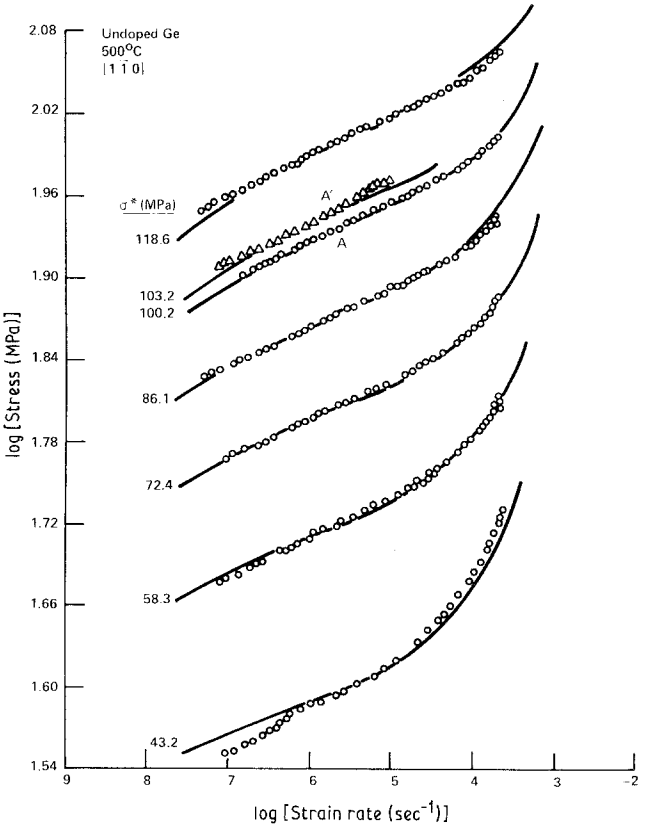

Figure 6 Log σ–log $\dot{\epsilon}$ data obtained from load relaxation experiments at several plastic strain levels for a high-purity germanium crystal compressed along $[1\bar{1}0]$ at 500° C. The solid curves are a fit of the data to the constitutive equations discussed in the text.

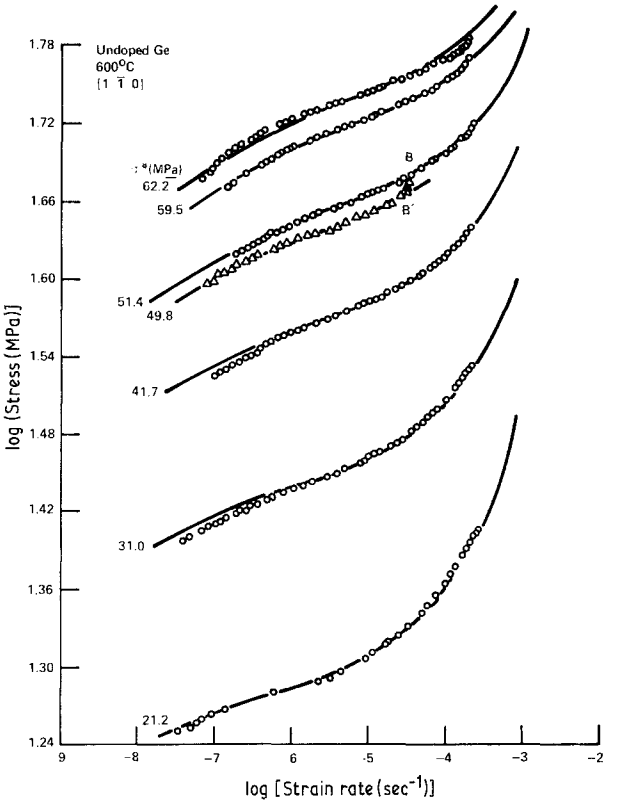

Figure 7 Log σ–log $\dot{\epsilon}$ data obtained from load relaxation experiments at several plastic strain levels for a high-purity germanium crystal compressed along [1$\bar{1}$0] at 600° C. The solid curves are a fit of the data to the constitutive equations discussed in the text.

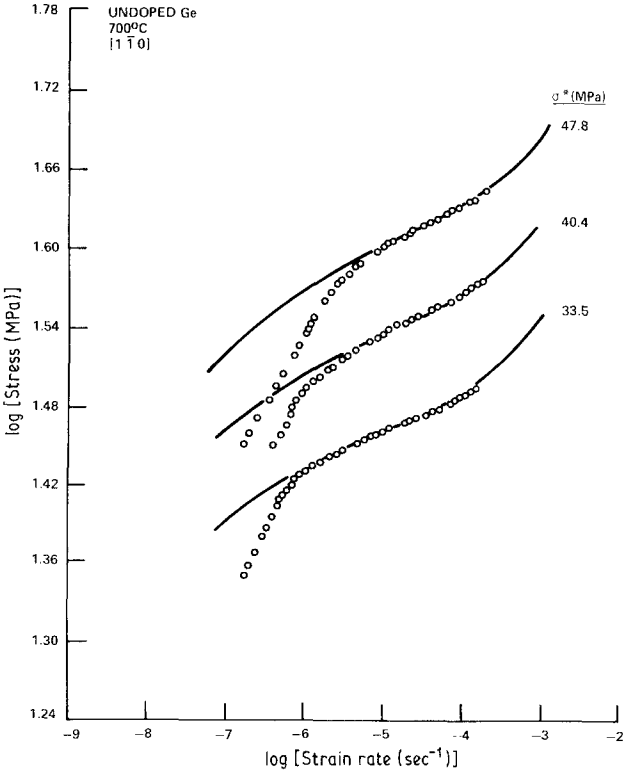

Figure 8 Log σ–log $\dot{\epsilon}$ data obtained from load relaxation experiments at three plastic strain levels for a high-purity germanium crystal compressed along [1$\bar{1}$0] at 700° C. The solid curves are a fit of the data to the constitutive equations discussed in the text.

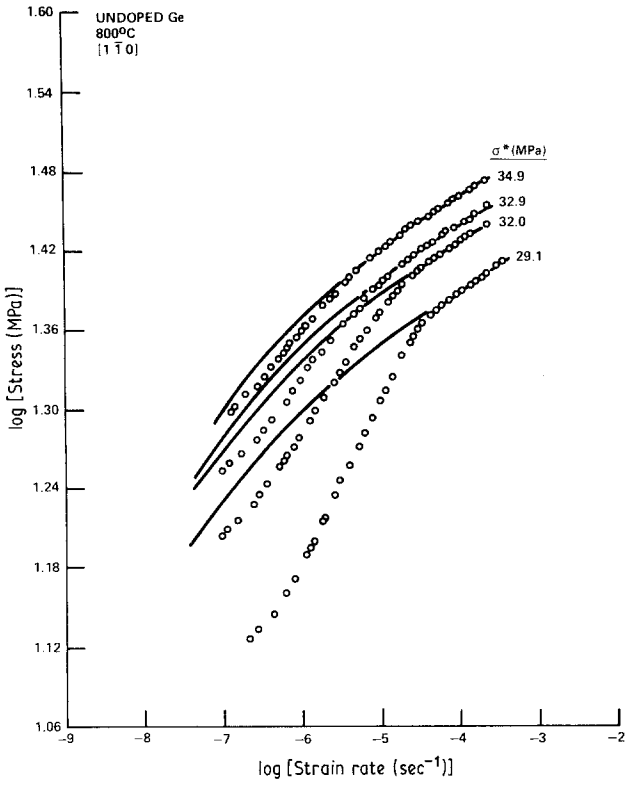

Figure 9 Log σ–log $\dot{e}$ data obtained from load relaxation experiments at four plastic strain levels for a high-purity germanium crystal compressed along [1$\bar{1}$0] at 800° C. The solid curves are a fit of the data to the constitutive equations discussed in the text.

polished, as-received (i.e. not predeformed and annealed) crystal relaxed from stress levels below the yield stress are presented in Fig. 4. During the first few minutes of the relaxation run, the strain rate increased as the stress decreased. This strain rate increase appears as a concave downward section of a load–time curve. To explore the cause of this behaviour, load relaxation tests on three crystals were interrupted at approximately the stress levels indicated in Fig. 4; these crystals were etched to reveal the following evolution of the dislocation structure. At the start of the test, the dislocation density was $\sim 10^3\,\mathrm{cm}^{-2}$. Dislocations are initially generated at the surfaces which contact the pistons (upper arrow, Fig. 4). The dislocation density increases rapidly approaching $\sim 10^8\,\mathrm{cm}^{-2}$ within a few seconds (middle arrow). After two hours (lower arrow), the dislocation distribution is nearly homogeneous and the density remains $\sim 10^8\,\mathrm{cm}^{-2}$. The rapid dislocation multiplication or slip band propagation in the early part of the test enables the strain rate to increase even though the stress, and thus the dislocation velocity, are decreasing. This point is clearly seen by considering the Orowan relation between strain rate, dislocation density ρ, dislocation velocity v, and Burger's vector $\mathbf{b}$: $\dot{e} = \rho \mathbf{b} v$. In the early part of a relaxation run, the small decrease in dislocation velocity or applied stress is more than offset by the large increase in dislocation density in certain parts of the specimen.

Several log σ–log $\dot{e}$ curves at 600° C, Fig. 7, which were obtained from the relaxation portions of the 600° C load-history shown in Fig. 1, vary from concave upward to concave downward as the strain level increases. The overall slopes of these concave upward curves decrease with increasing stress or strain. Similar behaviour was observed at 500 and 700° C, Figs. 6 and 8. This change in curvature with strain or stress level is similar to that observed in metals [23–27] and alkali halides [17–19].

3.3. Dislocation structures

The dislocation structures in the deformed germanium crystals vary markedly with temperature and stress. Optical micrographs of the dislocation structures revealed by etch pitting are presented in Fig. 10 for samples deformed at four different temperatures as described in Fig. 2. At 500° C, Fig. 10a, slip bands are observed. At 600° C, Fig. 10b, a lower density of these slip

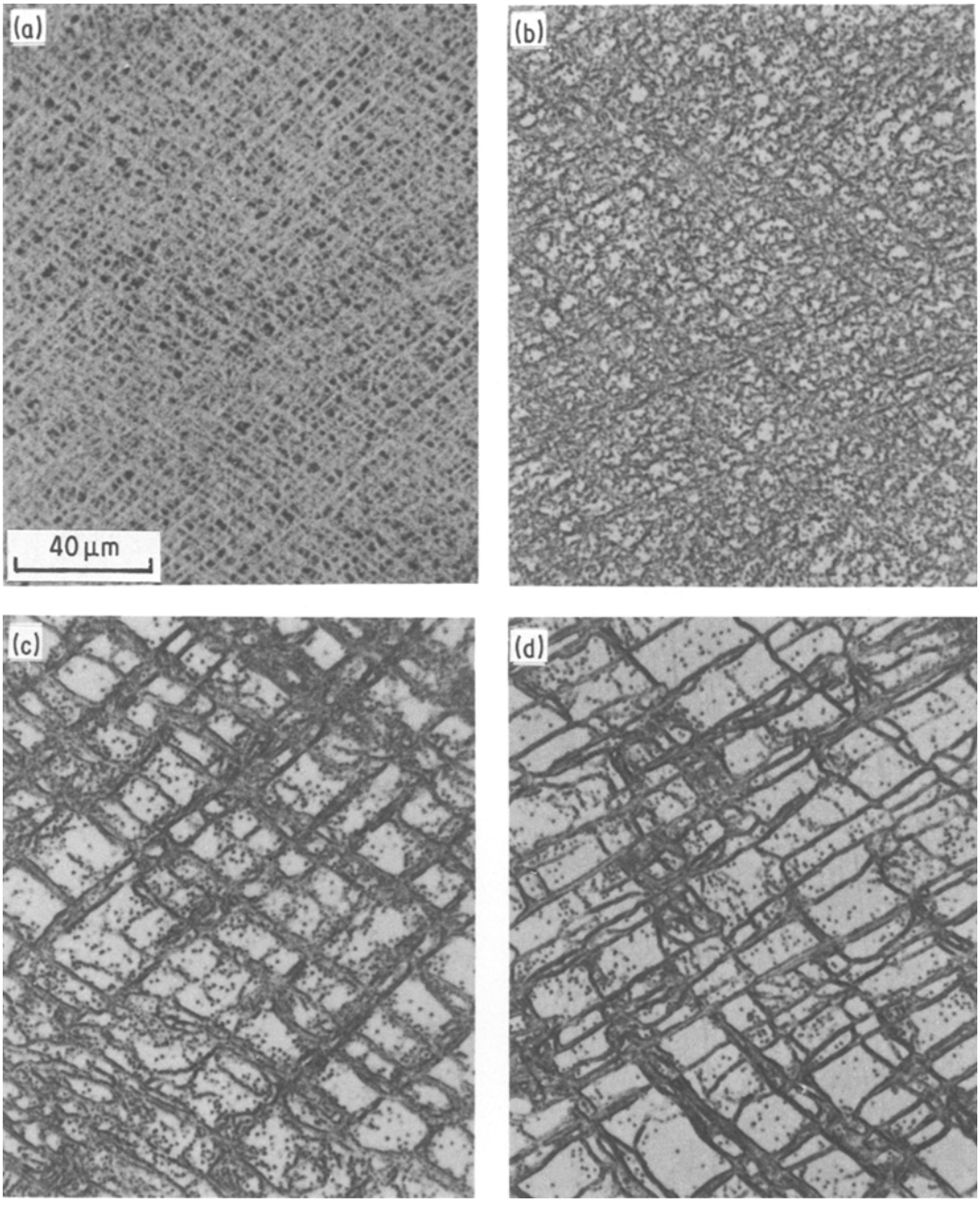

Figure 10 Dislocation structure revealed as etch pits on (111) surfaces of samples deformed at four temperatures as described in Fig. 2. The compression axes are vertical: (a) is for 500° C, (b) for 600° C, (c) for 700° C, and (d) for 800° C.

bands is found. The dislocations at 500 and 600° C are difficult to count in Figs. 10a and b, because the spacing between etch pits is below the resolution of the optical microscope. Dislocation cell structures are formed at 700 and 800° C. At 800° C, Fig. 10d, the cell size is ~ 20 μm, which is approximately twice as large as that of 700° C, Fig. 10c. The thickness of cell walls and the density of free dislocations between these walls are reduced as temperature is increased.

At 500° C, the dislocation structure observed in the TEM is characterized by a high density

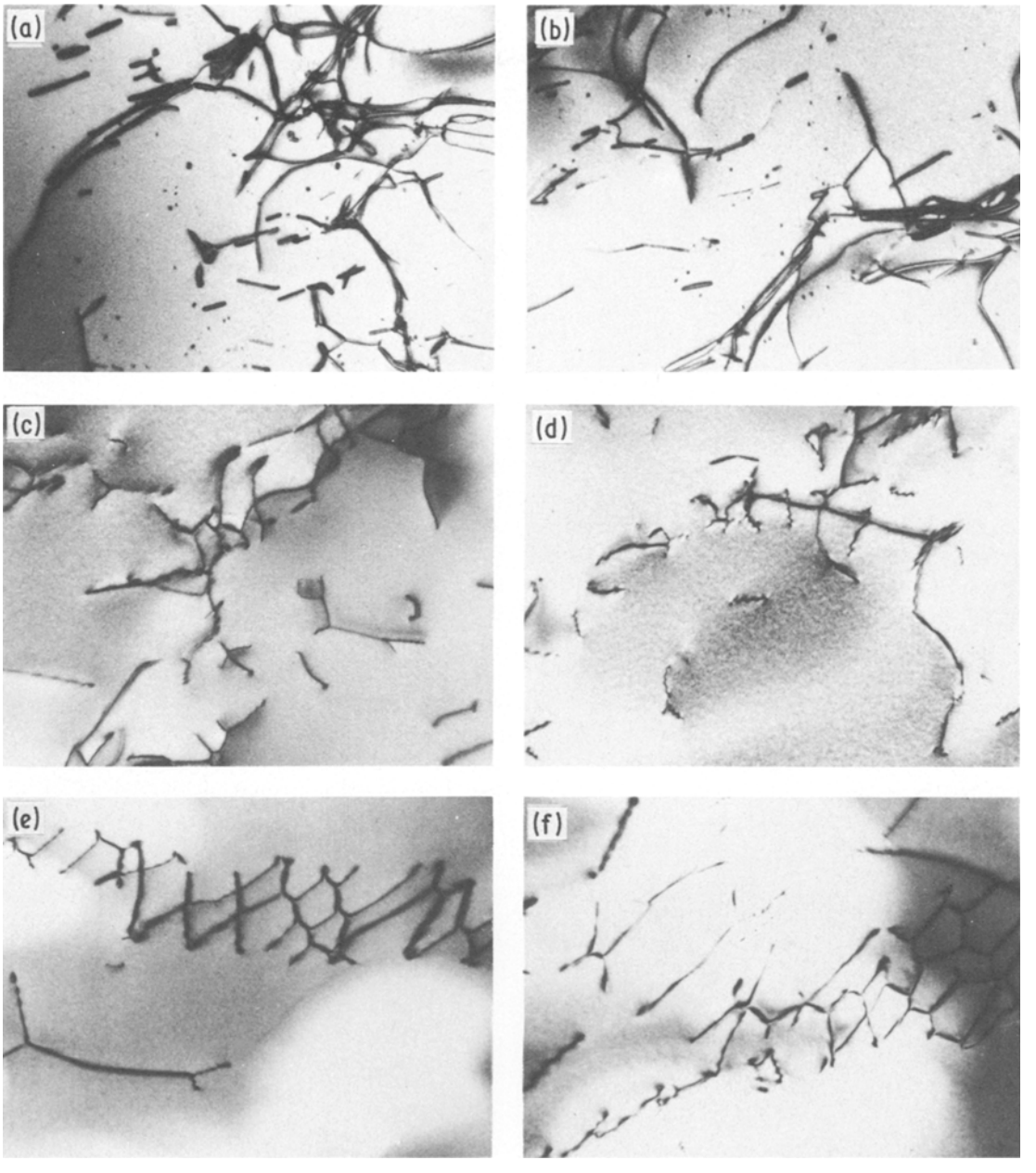

Figure 11 TEM micrographs of dislocation structures in (1 1 1) slip planes of samples deformed as described in Fig. 2. (a) and (b) are for 500° C, (c) and (d) for 600° C, (e) and (f) for 700° C, and (g) and (h) for 800° C.

($\sim 10^9$ cm^{-2}) of isolated and clustered dislocations, as well as dislocation dipoles, Figs. 11a and b. This microstructure, which is associated with the concave upward log σ–log $\dot{\epsilon}$ curves, suggests that a dislocation glide mechanism is predominant at this temperature. At 600° C, Figs. 11c and d, dislocations are more curved than at 500° C and cell structures are beginning to form.

At 700° C, most of the dislocations are organized into low angle boundaries, such as shown in Figs. 11e and f, with an average separation of about 10 μm. At 800° C, the dislocation structure is similar to that observed at 700° C, Figs. 11g and h. Again, the structure is dominated by well-developed low angle boundaries. This microstructure is typical of those produced by diffusion controlled deformation processes and is associated with the concave downward log σ–log $\dot{\epsilon}$ curves.

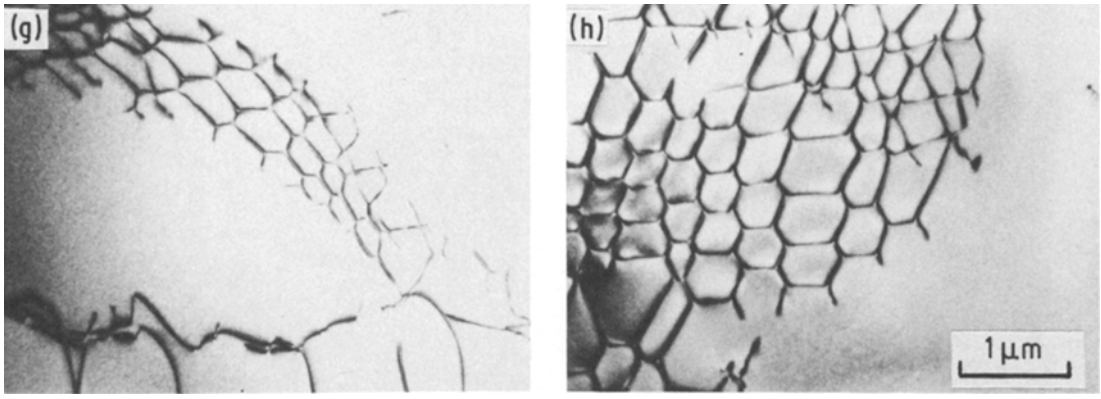

A dislocation cell structure dominates the microstructure of germanium crystals deformed at 800° C, Figs. 10d and 11g and h. To examine the extent to which the dislocation structure changes during a relaxation experiment at 800° C, the microstructure of a crystal deformed to 6% strain at $\dot{\epsilon} = 2 \times 10^{-4}\,\mathrm{sec}^{-1}$ and relaxed for 2 h was compared with that of a crystal loaded under the same conditions but not relaxed. The resulting dislocation structures are quite different, Fig. 12. Both crystals exhibit well-developed networks or low-angle boundaries, that is, cell walls. However, the cell size after a 2 h relaxation run was approximately twice as large as that before the relaxation, 10 μm as compared to 20 μm. Also, the density of free dislocations (dislocations within the cells) and the thickness of cell wall are substantially reduced after the load relaxation test. No recrystallization was found in Laue back reflection patterns. Clearly, a large amount of recovery has occurred during the relaxation test. This observation agrees with the observed decrease in yield point relative to the peak stress level from the previous loading at the higher temperatures, Fig. 2; it may also account for the S-shape of the $\log \sigma$–$\log \dot{\epsilon}$ curves, Fig. 9.

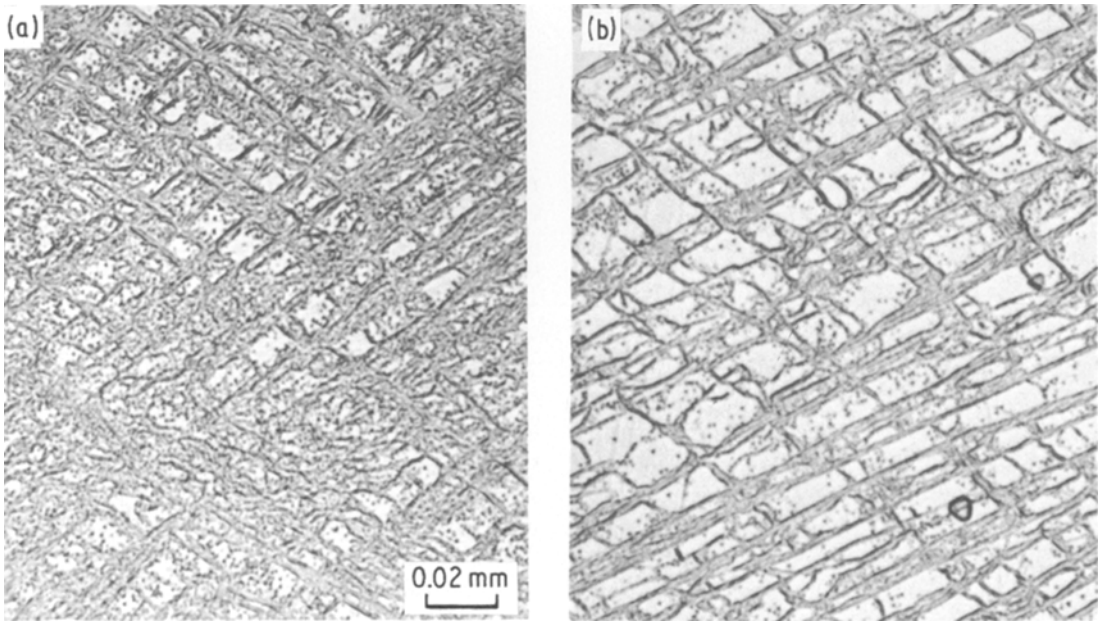

Figure 12 Comparison of dislocation structures revealed by etching samples on (1 1 1) which were deformed at 800° C (a) to 6% strain and (b) to 6% strain and then relaxed for 2 h.

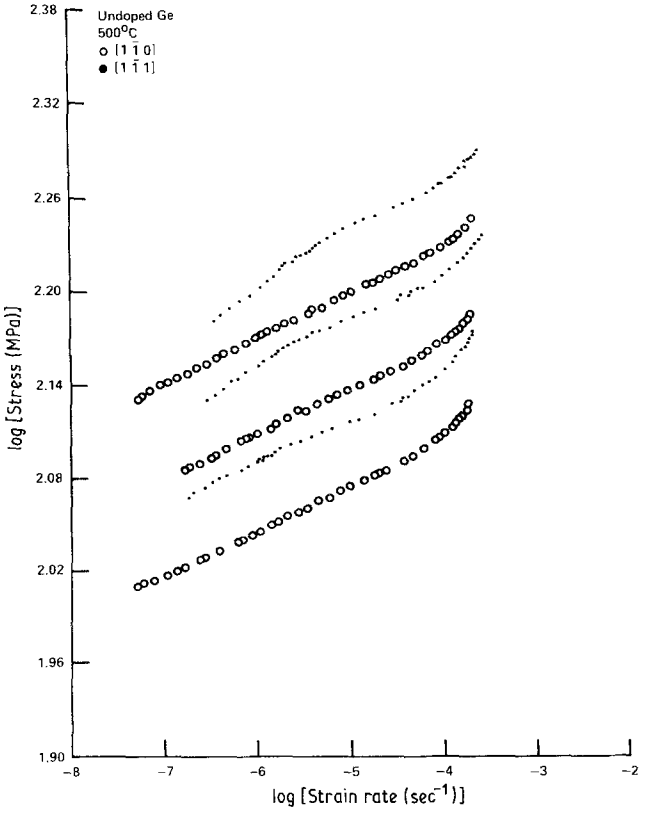

Figure 13 Log σ–log $\dot{\epsilon}$ data obtained from load relaxation experiments at three plastic strain levels for high-purity germanium crystals compressed along $[1\bar{1}1]$ and $[1\bar{1}0]$ at 500° C.

3.4. Effects of orientation and dopant level

Two crystals with $[1\bar{1}1]$ compression axes were deformed for comparison with the $[1\bar{1}0]$ samples. At 500° C, the log σ–log $\dot{\epsilon}$ curves for these two orientations are quite similar, Fig. 13. To compare data for the two orientations, the stresses measured for the $[1\bar{1}0]$ orientation were multiplied by the ratio of the Schmid factors, 0.41/0.27, for the $[1\bar{1}1]$ and $[1\bar{1}0]$ orientations. The data are concave upward for both orientations at the higher strain rates; however, the data for the $[1\bar{1}1]$ orientation turned markedly concave downward at the lower strain rates or higher stress level.

At 500° C, the log σ–log $\dot{\epsilon}$ data from load relaxation tests on heavily doped germanium (doping level $\sim 2 \times 10^{19}$ cm^{-3}) are concave upward, while those for intrinsic germanium are concave downward at the same applied stress level, as is shown in Fig. 14. Both samples had $[1\bar{1}1]$ compressive axes.

4. Mechanical equations of state

A mechanical equation of state is a functional relationship among the internal state parameters of the material (such as dislocation density and cell size) and the externally measurable variables (such as stress, strain rate and temperature). At least one internal state variable is required to predict the mechanical response of the materials from an equation of state. One method for developing a mechanical equation of state is the microstructual or mechanistic approach. If our physical understanding of the mechanisms of plastic flow and their dependence on the microstructure of the material were complete, then the accurate equation of state could be constructed. Such an equation would permit one to predict the macroscopic properties from microstructual observations and to prescribe the macroscopic behaviour by controlling the microstructure.

An alternative approach, the phenomenological approach, is to determine the relations between internal and external variables during inelastic deformation by well chosen experiments; that is, one might quantitatively characterize the material state by phenomenological parameters rather than by microstructural features. Such a phenomenological method of attack might provide an equation of state which could be used to correlate data from various types of mechanical tests, to extrapolate to conditions unattainable in the laboratory, and to reduce the amount of mechanical testing

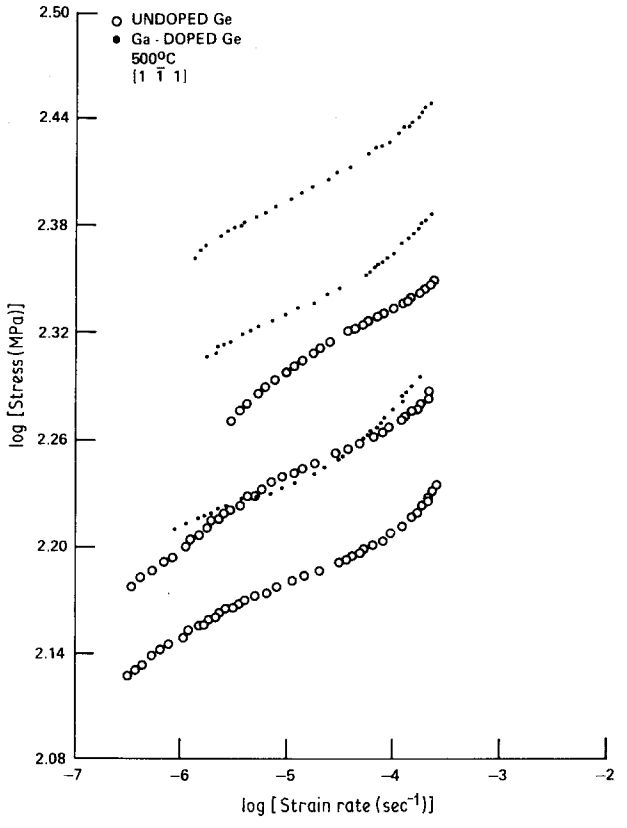

Figure 14 Log σ–log $\dot{\epsilon}$ data obtained from load relaxation experiments at three plastic strain levels for high-purity (undoped) and gallium-doped germanium crystals compressed along $[1\bar{1}1]$ at 500° C.

required to describe the current state and future behaviour of the material. In addition to providing constitutive relations important in mechanical design, the form and behaviour of an experimentally derived equation of state should provide a basis to further the fundamental understanding of plastic deformation processes by correlating them with associated microstructures.

Early attempts to formulate an equation of state for inelastic deformation were unsuccessful because they included not only state variables but also history variables such as strain and time which specify differences with respect to some initial state [28]. Different histories may result in the same microstructure and, thus, in the same properties. So the current deformation properties are uniquely determined by the current microstructure which defines the current material state.

Recently, several mechanical equations of state have been proposed. Hart [16, 29] built a three-element model to describe inelastic deformation in metals. Kocks [30, 31] reported constitutive relations for dislocation glide. Rohde and Swearengen [32, 33] used a power law and reaction rate theory to discuss a mechanical equation of state. Sherby *et al.* [34] and many other investigators used subgrain size as a state variable. Gupta and Li [35, 36] have used the internal stress as a state parameter.

4.1. Microstructural approach

One relationship used as an equation of state by several investigators is the power-law relation between stress, σ, and strain rate, $\dot{\epsilon}$. This power-law relation, which is frequently used to describe the macroscopic deformation behaviour of germanium, is based on the observed stress–dislocation velocity relation [3, 4]. The usual starting point for developing a σ–$\dot{\epsilon}$ relation from σ–v relation is the Orowan equation [37] which relates the strain rate to the dislocation density, ρ, and the mean dislocation velocity, v,

$$\dot{\epsilon} = \phi\rho\mathbf{b}v \qquad (1)$$

where ϕ is a geometrical factor and $\mathbf{b}$ is the dislocation Burger's vector. Paralleling the double-etching studies of Johnston and Gilman [38], the first measurements of the dislocation velocity in germanium reported that the dislocation velocity was proportional to the shear stress on the glide

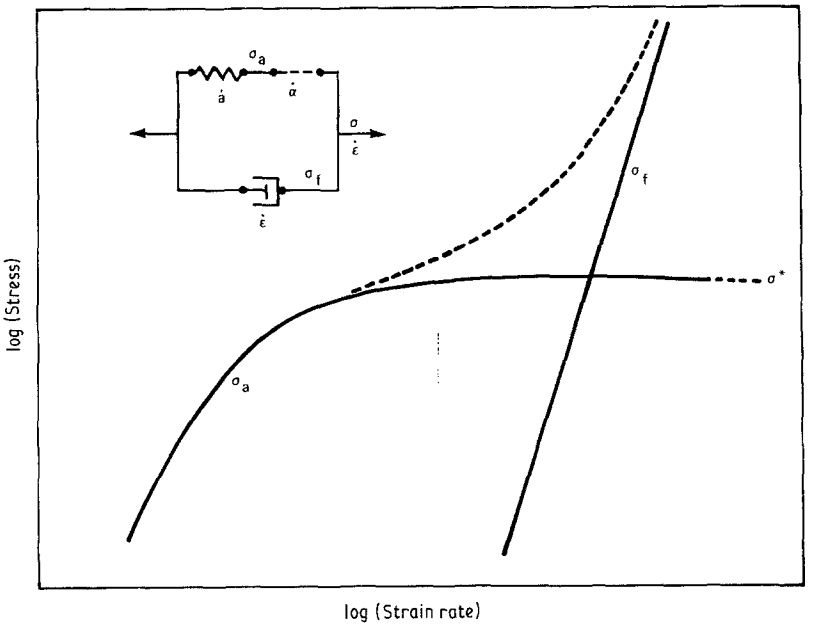

Figure 15 Log σ–log $\dot{\epsilon}$ curve predicted by the constitutive equations which describe the two branch rheological model shown in the upper left and discussed in the text [14].

plane, τ, raised to the power n [1, 39, 40]

$$v = B(T)\tau^n \tag{2}$$

where $B(T)$ is a function of temperature. In general, τ can be expressed in terms of the effective stress, σ_e,

$$\sigma_e = \sigma - \sigma_i \tag{3}$$

where σ is the applied stress and σ_i is the internal stress. The internal stress is generally assumed to be proportional to the square root of the dislocation density $\sigma_i \propto \rho^{1/2}$ [41]. For germanium, early investigations found that $n \simeq 1$ and that

$$B(T) = B_0 \exp(-U/kT) \tag{4}$$

where B_0 is a constant, $U \simeq 1.6\,\text{eV}$ is in good agreement with the energy calculated for the formation of a double kink, and kT has the usual meaning [39, 40, 42, 43]. When combined, these four equations yield an equation of state, with σ_i as a state variable, for plastic flow of the following form,

$$\dot{\epsilon} = B_0' \rho \mathbf{b} (\sigma - \sigma_i)^n \exp(-U/kT) \tag{5}$$

On a log σ–log $\dot{\epsilon}$ plot, Equation 5 predicts concave upward curves for $\sigma_i > 0$ and straight lines for $\sigma_i = 0$. Similar behaviour would be observed on a log σ–log v plot.

4.2. A phenomenological approach

Load relaxation studies by Lee and Hart [23] and others [24–27] have yielded a substantially more complex behaviour for metals. At low temperatures, high strain rates, and low hardness levels, the deformation response is prediced by Equation 5. However, at higher temperatures, and/or lower strain rates, the log σ–log $\dot{\epsilon}$ curves become concave downward. The same behaviour has been observed for the alkali halides and for silver chloride [17–19].

Similar behaviour might be anticipated for other crystalline solids and, in particular, for germanium. The most recent studies of dislocation velocity as a function of stress and temperature in germanium show a distinct transition from concave upward to concave downward log σ–log v curves when the temperature is increased from 440 to 580° C [4].

The observed inelastic, grain–matrix deformation behaviour for a variety of metals has been modelled by Hart in terms of three elements whose mutual relationship is described by the rheological diagram in Fig. 15 [16]. The stress in the upper branch, σ_a, acts on two elements; physically, the $\dot{\alpha}$-element might correspond to processes such as dislocations cutting through or climbing around barriers and the $\dot{a}$-element to processes which store elastic strain energy such as the piling up of dislocations. The stress in the lower branch, σ_f, acts on the $\dot{\epsilon}$-element which represents the frictional resistance of the lattice. As suggested by the diagram in Fig. 15, the stress and the strain

rate are constrained by the relations

$$\sigma = \sigma_a + \sigma_f \quad (6)$$

$$\dot{\epsilon} = \dot{a} + \dot{\alpha} \quad (7)$$

The $\dot{a}$-element is a linear element with a modulus $\mathscr{M}$ such that

$$\sigma_a = \mathscr{M} a \quad (8)$$

For metals, the high-temperature, $\dot{\alpha}$-element satisfies the relations

$$\sigma_a = \sigma^* \exp\left[-(\dot{\epsilon}^*/\dot{\alpha})^{\lambda}\right] \quad (9)$$

$$\dot{\epsilon}^* = (\sigma^*/G)^m f \exp(-Q/kT) \quad (10)$$

$$d\ln\sigma^*/dt = \Gamma(\sigma_a, \sigma^*)\dot{\alpha} - R(\sigma^*, T) \quad (11)$$

In these equations, λ, m, f and Q are materials constants; G is the elastic shear modulus; Γ and R describe work hardening and recovery, respectively; $\dot{\epsilon}^*$ is a rate parameter which is related to the state variable (hardness parameter) σ^* through Equation 10. The $\dot{\epsilon}$-element, which dominates at lower temperatures, higher strain rates, and lower hardness levels, is described by

$$\sigma_f = \mathscr{M}(\dot{\epsilon}/\dot{a}^*)^{1/M} \quad (12)$$

where $\dot{a}^*$ is a temperature dependent rate parameter, $\dot{\epsilon}$ has the same sign as σ_f, and M is a materials parameter.

If Equations 9 and 10 describe the experimental results, then the log σ–log $\dot{\epsilon}$ data collected at various hardness levels will form a series of concave downward curves which can be superimposed by translation along a line of slope $1/m$. If the results follow Equation 12 and if $\sigma_a \simeq \sigma^*$, then the log σ–log $\dot{\epsilon}$ curves at various hardness levels will be concave upward. These curves, too, can be superimposed, now by translation along a line of slope $1/M$.

When the plastic strain, and thus the strain hardening, during a load relaxation test is very small, the measured stress–strain rate curves describe the inelastic deformation behaviour at constant structure or hardness, provided that recovery is minimal. In some of the analyses of the data for metals [27], the anelastic term, $\dot{a}$, has been ignored as a first approximation. In the present study, $\dot{a}$ is considered in the following manner: The combination of Equations 9 and 12 via Equation 6 gives

$$\sigma = \sigma^* \exp\left[-(\dot{\epsilon}^*/\dot{\alpha})^{\lambda}\right] + \mathscr{M}(\dot{\epsilon}/\dot{a}^*)^{1/M} \quad (13)$$

An expression for $\dot{\alpha}$ can be obtained from Equations 6 and 7 and the derivatives of Equations 8 and 12

$$\dot{\alpha} = \dot{\epsilon} - \left\{\dot{\sigma} - \left[\frac{\mathscr{M}}{M}\left(\frac{\dot{\epsilon}}{\dot{a}^*}\right)^{\frac{1-M}{M}} \frac{\ddot{\epsilon}}{\dot{a}^*}\right]\right\} \frac{1}{\mathscr{M}} \quad (14)$$

Equations 13, 14 and 10 were used to fit the load relaxation σ, $\dot{\epsilon}$ data in this study. The functional form of the change of hardness with time, Equation 11, during the load relaxation test is not known. Thus, only the portion of the data for any given run for which the hardness is approximately constant is fitted.

5. Application of a one-state-variable deformation model

The macroscopic mechanical behaviour of germanium during load relaxation tests, as described in Section 3, can be summarized as follows. The curvature of log σ–log $\dot{\epsilon}$ data changes from concave upward to concave downward as the test temperature increases or as the strain level increases at fixed temperature. Similar behaviour in metals was used by Hart [16] to construct a one-state-variable deformation model. In terms of this model, when the applied stress is higher than the hardness state of the material, the log σ–log $\dot{\epsilon}$ relationships are concave upward; when the applied stress is smaller than the hardness level, the curvature becomes concave downward. The two major plastic deformation mechanisms suggested by this model are dislocation glide and dislocation climb, respectively, which are represented by the $\dot{\epsilon}$ and $\dot{\alpha}$ elements in the rheological model in Fig. 15.

Analytical equation for softening and hardening phenomena were not introduced into Hart's deformation model [16]; thus, the constant hardness behaviour is of major interest here. At 800° C, the hardness state in germanium clearly recovers during a load relaxation test. In this situation, only the high strain rate data are considered under the assumption that little recovery occurred in the first few seconds of a relaxation test.

The following comments can be made, based on Figs. 2 and 3, concerning strain-ageing or hardening during load relaxation tests. At 500° C: (a) the source of the yield drop is uncertain. It may be due to dislocation multiplication. However, it may reflect impurity (e.g. oxygen), pinning of the dislocations [44, 45], atomic rearrangement at the dislocation core [46] and/or barrier or drag forces resulting from stair-rod or Cottrell–Lomer

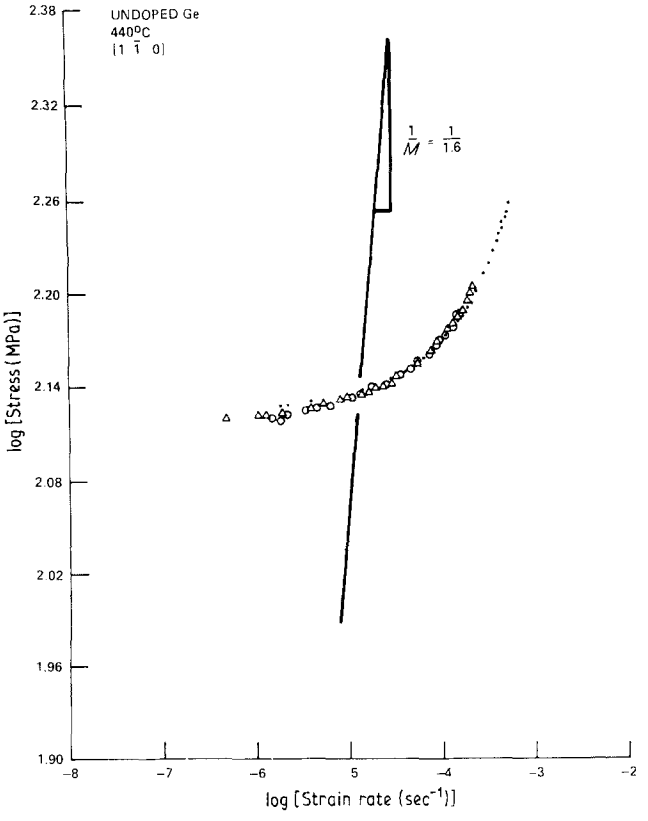

Figure 16 Log σ–log $\dot{\epsilon}$ data at 440° C, from Fig. 5, obtained at three plastic strain levels translated along a line of slope $M^{-1} = (1.6)^{-1}$ to give a single master curve.

dislocations [47] or jogs on dislocation dipoles [48] which are prevalent at 500° C as shown in Fig. 11. (b) The fact that the yield drop is larger when preceded by a relaxation run, than when preceded by a simple loading–unloading run, suggests that some time-dependent immobilization of the dislocations must occur during the load relaxation test. (c) The hardening indicated by the fact that the reloading lower yield point exceeds the previous peak stress probably occurs during reloading, and not during load relaxation. This point is supported by the 500° C relaxation runs, described below, in which the sample was loaded to below the yield point.

Except for the recovery and hardening phenomena discussed above, the following assumption is made before fitting log σ–log $\dot{\epsilon}$ data to Hart's model. The dislocation structure is well developed by predeformation beyond the yield point; the rapid dislocation multiplication at 400° C does not occur at higher temperatures.

5.1. Curve fitting log σ–log $\dot{\epsilon}$ data

All three elements (a, $\dot{\alpha}$, $\dot{e}$) of Hart's rheological model, Fig. 15, were used to fit the experimental data. The material constants λ, M and m were assumed to be independent of temperature, stress, strain rate and hardness state. For the 400, 440, 500 and 600° C data, the concave upward part of the log σ–log $\dot{\epsilon}$ curves could be superimposed onto a single curve translation along a line of slope $1/M$. Translation of the 440° C curves onto a single curve, Fig. 16, yielded $M = 1.6 \pm 0.2$. Similarly, translation of the concave downward part of log σ–log $\dot{\epsilon}$ curves at 700, 800 and 885° C gave $m = 3.4$. The range of possible values for λ was determined by curve fitting the concave downward part of the log σ–log $\dot{\epsilon}$ data. The value of the parameters, M, m and λ for seven temperatures are presented in Table I. Values of $M = 1.6$ and $m = 3.4$ were used in all of the curve fitting described below. Because the relatively high values of λ obtained at the higher temperatures may be caused by recovery, $\lambda = 0.15$ was chosen.

An iterative least squares fit to a nonlinear function [49] was used to find $f \exp(-Q/RT)$, $\dot{a}^*$ and $\mathcal{M}$ for every temperature and σ^* for every run. The data were fitted to Equations 10 and 13 including the $\dot{a}$-element with the use of Equation 14. Values for the parameters $f \exp(-Q/RT)$,

TABLE I Values for the parameters M, m and λ for germanium

T(° C)	M	m	λ
400	2.0 ± 0.5	–	–
440	1.6 ± 0.2	–	–
500	2.5 ± 0.3	–	0.1 ± 0.05
600	2.2 ± 0.3	–	0.3 ± 0.1
700	–	3.3 ± 0.5	0.5 ± 0.2
800	–	3.6 ± 0.5	0.4 ± 0.2
885	–	3.2 ± 0.5	–

$\mathscr{M}$, and $\dot{a}^*$ from the curve fitting are listed in Table II for four temperatures. Values of the elastic shear modulus G for the (1 1 1) [1 $\bar{1}$ 0] slip system were calculated from data in [50] with the method in [51].

The curves drawn in Figs. 6 to 9 are the results of the fitting procedure. The deviation of the high strain rate data at 500° C from the curves is believed to be due to strain hardening and inhomogeneous deformation. At 600° C, Fig. 7, the deviation of the data from the predicted curve at strain rates less than 10^{-6} sec^{-1} may be caused by recovery. S-shaped log σ–log $\dot{\varepsilon}$ curves, similar to those shown in Fig. 9 for germanium at 800° C, have been observed for some metals (e.g. lead) [52]. One possible explanation for this behaviour is that a new mechanism, such as grain boundary sliding, becomes important at the higher temperatures and lower strain rates. Subgrain boundaries are well developed under these conditions in germanium; however, Laue back reflection patterns show no signs of recrystallization. Thus, only dynamic recovery, and not recrystallization and grain boundary sliding, can be associated with the observed change in curvature.

For the load relaxation run A′ at 500° C, shown in the stress–strain curves of Fig. 2, the sample was reloaded to a stress less than the peak stress of the previous relaxation run A. The log σ–log $\dot{\varepsilon}$ curves for A and A′ are presented in Fig. 6. The log σ–log $\dot{\varepsilon}$ curve for A′ lies at a slightly higher hardness level than that for run A. This result suggests that some hardening takes place before the sample macroscopically yields or that strain-ageing occurs during relaxation. This conclusion is supported by the relative positions of the lower yield point and the previous peak stress discussed in the section on stress–strain curves.

A loading–reloading pair of relaxation runs, B and B′, were also obtained at 600° C, Figs. 2 and 7. The observation is that the reloading curve joins onto the low strain rate portion of the preceeding run indicating that recovery is minimal.

5.2. Discussion of parameters

The three parameters, $f \exp(-Q/RT)$, $\dot{a}^*$, and $\mathscr{M}$, are plotted against inverse temperature in Fig. 17. The parameter $f \exp(-Q/RT)$ changes slope near 550° C. Below 550° C, $Q \simeq 0.5$ eV, and above 550° C, $3 \leqslant Q \leqslant 4.3$ eV. The low apparent activation energy at the lowest temperatures and highest stresses suggests that mechanisms such as cutting of barriers by dislocations are important. For example numerous jogs, which appear as constrictions between two Shockley partial dislocations, were observed in weak-beam images of the 500° C samples [53, 54]. Some thermal activation is needed for a kink to move past a jog, which thus acts as a weak barrier to dislocation glide. The higher apparent activation energy at the highest temperatures is similar to those for self-diffusion and cross-slip in germanium, 2.97 [55] and 4.5 eV [56], respectively. Thus, the physical mechanism associated with the $\dot{\alpha}$-element is that of dislocation motion around barriers by climb or cross-slip at temperatures above 600° C.

The $\dot{a}^*$ parameter measures the mobility of dislocations. For covalent materials such as germanium, kink formation is believed to strongly influence dislocation mobility. The increase in the slope of $\dot{a}^*$ against $1/T$ with increasing temperature, Fig. 17, is consistent with Möller's [14] conclusion from dislocation velocity studies that the kink formation energy increases with increasing temperature.

At any given temperature, a single value of $\mathscr{M}$ is adequate to curve fit the data, suggesting that $\mathscr{M}$ is not strongly stress dependent. The temperature dependence of $\mathscr{M}$ is shown in Fig. 17. At 500° C,

TABLE II Values of the parameters $f \exp(-Q/RT)$, $\mathscr{M}$, $\dot{a}^*$ and G for germanium

T(° C)	$f \exp(-Q/RT)$ (sec^{-1})	$\mathscr{M}$ (MPa)	$\dot{a}^*$ (sec^{-1})	G (MPa)
500	0.011	1.58×10^4	25.7	4.448×10^4
600	0.063	0.79×10^4	31.6	4.381×10^4
700	2.5	0.50×10^4	63.1	4.312×10^4
800	158.5	0.32×10^4	100.0	4.230×10^4

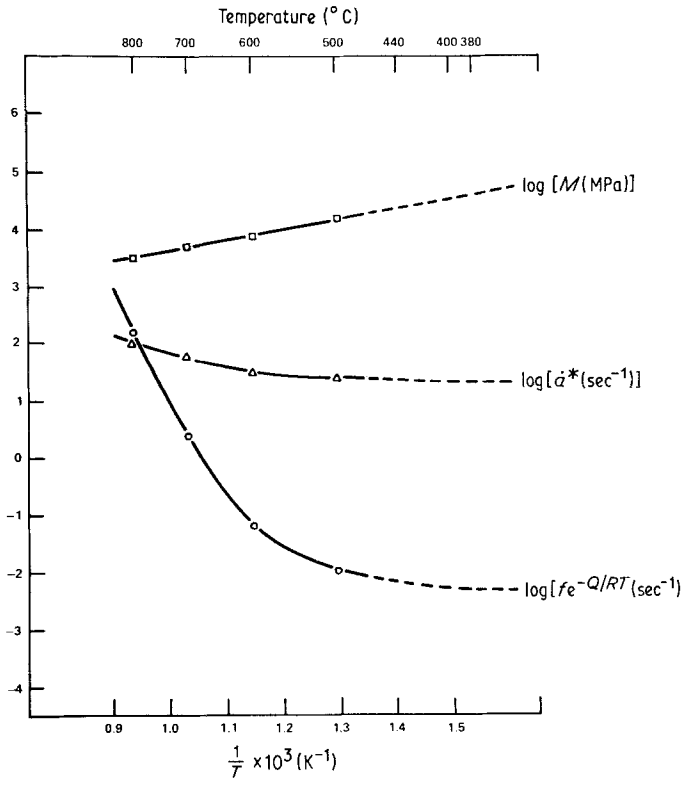

Figure 17 Log of each of the three parameters $f \exp(-Q/RT)$, $\dot{a}^*$ and $\mathscr{M}$ against inverse temperature. Values for the three parameters were obtained by curve fitting the load relaxation data at 500, 600, 700 and 800° C to Equations 10, 13 and 14.

$\mathscr{M} \simeq 1/3G$ and at 800° C, $\mathscr{M} \simeq 1/13G$. An apparent activation energy of 0.4 ± 0.2 eV is obtained, if an Arrhenius relation between $1/\mathscr{M}$ and T is used.

The extrapolated values of parameters $\dot{a}^*$, $\mathscr{M}$ and $f \exp(-Q/RT)$ as shown in Fig. 17 were used to fit the load relaxation data at 400° C. As demonstrated in Fig. 4, the low strain rate data can be described by these parameters; while the high strain rate data cannot be fitted well. The deviation of the data in the early (high strain rate) part of relaxation is consistent with an increasing dislocation density in the course of relaxation as discussed with reference to Fig. 4.

5.3. Load relaxation and dislocation velocity data

To compare load relaxation results with published dislocation velocity–stress data [4], the material constants M, m and λ and the values of the parameters $\mathscr{M}, \dot{a}^*$ and $f \exp(-Q/RT)$ extrapolated to 380° C were used to curve fit the log σ–log v data using the Orowan equation (Equation 1) with the dislocation density as a variable to be determined from the curve fitting. The log σ–log $\dot{e}$ curves at 380, 440 and 500° C predicted by our results and those obtained from log σ–log v data, which are presented in Fig. 18, are in good agreement. The values of ρ are reasonable for the applied stress levels. The value of σ^* are lower than those obtained from the load relaxation data.

Two questions arise from this analysis: (a) Why are the values for σ^* calculated from the σ–v data lower than the values determined from the σ–$\dot{e}$ data? (b) What is the relation between the values for σ^* and ρ listed in Fig. 18? First, the dislocation velocity data were obtained by measuring the glide velocity of isolated dislocations [4]. The only barrier to dislocation motion, in this case, should be the lattice friction (i.e. the Peierls barrier); dislocation–dislocation interactions are unimportant. Thus, the values of σ^* in Fig. 18 are associated with the Peierls potential. A plot of log σ^* against $1/T$ yields an activation energy of 0.25 ± 0.06 eV, which is in excellent agreement with the calculated Peierls potential for germanium [57]. This observation suggests that the hardness involved in the glide motion of free dislocations is closely associated with the Peierls potential. Second, two state variables, σ^* and ρ, were introduced in Fig. 18. These state variables are related by $\sigma^* \propto \rho^{1/3}$

It might be possible to relate the concept of hardness, σ^*, to the internal stress if the material

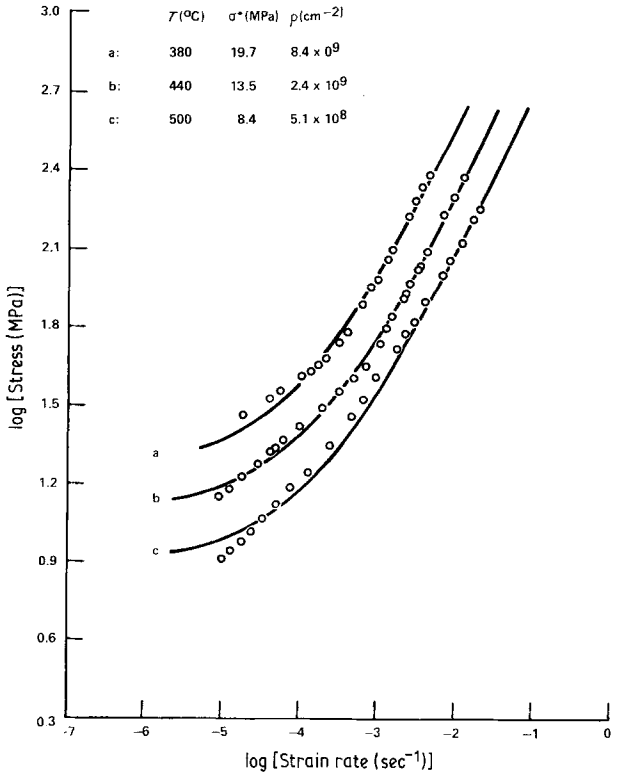

Figure 18 Log σ–log $\dot{\epsilon}$ points generated from published stress–dislocation velocity data compared with log σ–log $\dot{\epsilon}$ curves calculated from the constitutive equations with the parameters obtained in this study.

constants M, m and λ and the values of the parameters $\mathscr{M}$, $\dot{a}^*$ and $f \exp(-Q/RT)$ at 560 and 705° C in Fig. 17 are used to fit stress–velocity data shown in Fig. 10 of [5]. Following this approach, we found that the difference in σ^* between two dislocation densities at 560° C is nearly twice that of 705° C; this relation holds for internal stress as well [5].

5.4. The effect of doping with gallium

The glide velocity of dislocations in germanium highly doped with gallium is more than a factor of 3 lower than that in high purity germanium [58]. At comparable dislocation densities or hardness states, therefore, the low-temperature contribution to the constitutive equations, the σ_f curve in Fig. 15, should move to the left; the high-temperature contribution, the σ_a curve, will remain fixed. As a result, the 500° C log σ–log $\dot{\epsilon}$ curves for gallium-doped germanium should be more concave upward than those for undoped germanium at comparable stress levels. This behaviour is, in fact, exactly that observed, Fig. 14.

5.5. The effect of compression axis

Fig. 13 demonstrates that the log σ–log $\dot{\epsilon}$ data for samples compressed along $[1\bar{1}1]$ show a greater contribution from the high-temperature, concave downward branch (Fig. 15) of Hart's model than do the samples compressed along $[1\bar{1}0]$. This observation can be understood in the following manner. In the $[1\bar{1}1]$ samples, screw dislocations can readily cross-slip around obstacles (other dislocations) because two cross-slip planes are available for each Burgers vector. However, in the $[1\bar{1}0]$ samples, there is zero resolved shear stress on all potential cross-slip planes. Thus, while the contribution of the low-temperature branch should be similar for the two orientations, the high-temperature branch (which describes cross-slip and climb-type mechanisms) contributes more to the deformation of $[1\bar{1}1]$ samples than to the deformation of $[1\bar{1}0]$ samples; that is, the σ_a curve in Fig. 15 is moved to the right for the $[1\bar{1}1]$ orientation in comparison to the $[1\bar{1}0]$ orientation.

Acknowledgements

This work was supported by the Department of Energy under grant Number DE-AC02-77ER04441. The transmission electron microscope was made available through the Central Facility for Electron Microscopy in the Materials Science Centre at Cornell University.

References

1. H. ALEXANDER and P. HAASEN, *Solid State Phys.* **22** (1968) 27.
2. A. R. LANG, *J. Appl. Phys.* **29** (1958) 597.
3. H. SCHAUMBURG, *Phil. Mag.* **25** (1972) 1429.
4. J. R. PATEL and P. E. FREELAND, *J. Appl. Phys.* **42** (1971) 3298.
5. R. L. BELL and W. BONFIELD, *Phil. Mag.* 9 (1964) 9.
6. P. PENNING and G. DE WIND, *Physica* **25** (1959) 765.
7. D. J. H. COCKAYNE, I. L. F. RAY and M. J. WHELAN, *Phil. Mag.* **20** (1969) 1265.
8. I. L. F. RAY and D. J. H. COCKAYNE, *Proc. Roy. Soc. A* **325** (1971) 543.
9. *Idem, J. Microsc.* **98** (1973) 170.
10. F. HÄUSSERMANN and H. SCHAUMBURG, *Phil. Mag.* **27** (1973) 745.
11. A. GOMEZ, D. J. H. COCKAYNE, P. B. HIRSCH and V. VITEK, *ibid.* **31** (1975) 105.
12. C. B. CARTER and P. B. HIRSCH, *ibid.* **35** (1977) 1509.
13. K. WESSEL and H. ALEXANDER, *ibid.* **35** (1977) 1523.
14. H.-J. MÖLLER, *Acta Metall.* **26** (1978) 963.
15. A. S. ARGON (ed.), "Constitutive Equations in Plasticity" (MIT Press, Cambridge, Mass., 1975).
16. E. W. HART, *Trans. J. Eng. Mater. Technol.* **98** (1976) 193.
17. I. LERNER, S.-W. CHIANG and D. L. KOHLSTEDT, *Acta Metall.* **27** (1979) 1187.
18. I. LERNER and D. L. KOHLSTEDT, *J. Amer. Ceram. Soc.* **64** (1981) 105.
19. *Idem, Acta Metall.* **30** (1982) 225.
20. E. BILLIG, *Proc. Roy. Soc.* **A235** (1956) 37.
21. W. G. JOHNSTON, *J. Appl. Phys.* **33** (1962) 2716.
22. J. R. PATEL and A. R. CHAUDHURI, *ibid.* **34** (1963) 2788.
23. D. LEE and E. W. HART, *Metall. Trans.* **2** (1971) 1245.
24. E. W. HART and H. D. SOLOMON, *Acta Metall.* **21** (1973) 295.
25. H. YAMADA and C. Y. LI, *Metall. Trans.* **4** (1973) 2133.
26. *Idem, Acta Metall.* **22** (1974) 249.
27. F. H. HUANG, F. V. ELLIS and C. Y. LI, *Metall. Trans.* **8A** (1977) 699.
28. C. ZENER and J. H. HOLLOMAN, *J. Appl. Phys.* **17** (1946) 69.
29. E. W. HART, C. Y. LI, H. YAMADA and G. L. WIRE, in "Constitutive Equation in Plasticity", edited by A. S. Argon (MIT Press, Cambridge, Mass., 1975) p. 149.
30. U. F. KOCKS, *J. Eng. Mater. Technol.* **98** (1976) 76.
31. *Idem,* in "Constitutive Equations in Plasticity", edited by A. S. Argon (MIT Press, Cambridge, Mass., 1975) p. 81.
32. R. W. ROHDE and J. C. SWEARENGEN, *J. Eng. Mater. Technol.* **99** (1977) 59.
33. J. C. SWEARENGEN and R. W.ROHDE, *Metall. Trans.* **8A** (1977) 577.
34. O. D. SHERBY, R. H. KLUNDT and A. MILLER, *ibid.* **8A** (1977) 843.
35. I. GUPTA and J. C. M. LI, *ibid.* **1** (1970) 2323.
36. *Idem, Mater. Sci. Eng.* **6** (1970) 20.
37. E. OROWAN, *Proc. Phys. Soc. London* **52** (1940) 8.
38. W. G. JOHNSTON and J. J. GILMAN, *J. Appl. Phys.* **30** (1959) 129.
39. A. R. CHAUDHURI, J. R. PATEL and L. G. RUBIN, *ibid.* **33** (1962) 2736.
40. *Idem, ibid.* **34** (1963) 240.
(1963) 240.
41. S. TAKEUCHI and A. S. ARGON, *J. Mater. Sci.* **11** (1976) 1542.
42. S. SCHAFER, *Phys. Status Solidi* **19** (1967) 297.
43. O. W. JOHNSON, *J. Appl. Phys.* **36** (1965) 3247.
44. J. R. PATEL, *Discuss. Faraday Soc.* **38** (1964) 201.
45. A. H. COTTRELL, "Dislocations and Plastic Flow in Crystals" (Oxford University Press, London, 1953) p. 140.
46. H. NEUHÄUSER and H. FLOR, *Scripta Metall.* **12** (1978) 443.
47. J. P. HIRTH and J. LOTHE, "Theory of Dislocations" (McGraw Hill, New York, 1968).
48. U. F. KOCKS, A. S. ARGON and M. F. ASHBY, *Prog. Mater. Sci.* **19** (1975) 64.
49. P. R. BEVINGTON, "Data Reduction and Error Analysis for the Physical Sciences" (McGraw-Hill, New York, 1969) p. 237.
50. Y. A. BURENKOV, S. P. NIKANOROV and A. V. STEPANOV, *Sov. Phys. Solid State* **12** (1971) 1940.
51. R. F. S. HEARMON, *Rev. Modern Phys.* **18** (1946) 409.
52. G. L. WIRE, H. YAMADA and C. Y. LI, *Acta Metall.* **22** (1974) 505.
53. S.-W. CHIANG, C. B. CARTER and D. L. KOHLSTEDT, *Phil. Mag.* **42** (1980) 103.
54. *Idem, Scripta Metall.* **14** (1980) 803.
55. B. J. BOLTAKS, in "Diffusion in Semiconductors", translated by J. I. Carasso, edited by H. J. Goldsmid (Academic Press, New York, 1963) p. 93.
56. H.-J. MOLLER and P. HAASEN, *Phys. Status Solidi* **33a** (1976) K59.
57. R. LABUSCH, *ibid.* **10** (1965) 645.
58. J. R. PATEL and A. R. CHAUDHURI, *Phys. Rev.* **143** (1966) 601.

Received 27 February
and accepted 30 April 1984